ELSEVIER

Performance analysis and optimization of PEM fuel cell stacks using flow network approach

G. Karimi[1], J.J. Baschuk, X. Li*

Department of Mechanical Engineering, University of Waterloo, 200 University Avenue West, Waterloo, Ont., Canada N2L 3G1

Abstract

The performance of polymer electrolyte membrane (PEM) fuel cell stacks can be improved significantly by optimizing the design and operating conditions. In this study, performance modeling and optimization of a PEM fuel cell stack have been conducted. The pressure and molar flow rate distributions for the fuel and oxidant streams in the stack are determined with a flow network model incorporating the minor losses. The distributions are then used in the single cell model developed previously to evaluate the performance of PEM fuel cell stack. Analysis has been carried out for different fuel and oxidant flow configurations and bipolar plate designs. It was found that the minor losses increase the stack operating pressure and the power requirement for oxidant supply and alter the cell-to-cell voltage variations in the stack. A symmetric double inlet–single outlet topology provides optimal stack performance with reasonably low compressor power requirement for the reactant flow and minimum cell-to-cell voltage variations. The stack performance is considerably affected by the size and the number of flow channels on bipolar plate. Optimal stack performance requires the matching of the stack manifold designs, flow channels on the bipolar plates and the stack operating conditions.
© 2005 Elsevier B.V. All rights reserved.

Keywords: PEM fuel cell; Stack; Performance optimization; Flow network analysis; Mathematical modeling

1. Introduction

Polymer electrolyte membrane (PEM) fuel cells convert the chemical energy of hydrogen and oxygen directly and efficiently into electrical energy and are widely regarded as alternative stationary and mobile power source. The main characteristics of PEM fuel cells are: they produce water as a byproduct; they have higher efficiency when compared with heat engines; they operate at low temperatures (up to 90 °C), which allows a fast start-up; they use a solid polymer as the electrolyte, which reduces concerns related to construction, transportation, and safety. Before PEM fuel cells can be successfully commercialized, the production cost must be reduced from the current estimate of approximately $ 200/kW to $ 30/kW [1].

The output voltage of a single PEM fuel cell is limited, usually less than 1 V. In order to produce a useful voltage for practical applications, several unit cells are connected in series to form a fuel cell stack. The output voltage depends on the number of unit cells. Fuel and oxidant flow through the fuel cells in multiple channels arranged in a complex flow network. This produces major challenges for fuel cell designers since the flow distribution within a fuel cell stack could have a significant impact on fuel cell performance and efficiency, and the heat and water management strategies, which are successful for single PEM fuel cells, are difficult to implement in a stack environment. As a result, the efficiency and power output of a PEM fuel cell operating within a stack are lower than the performance of a PEM fuel cell operating independently [2].

Over the past few years, a significant amount of research has been devoted to the study of PEM fuel cell stacks and several empirical and mathematical models have been developed for the purpose of understanding and predicting PEM fuel cell performance. A comprehensive review of the published

* Corresponding author. Tel.: +1 519 888 4567x6843;
fax: +1 519 888 6197.
[1] Permanent address: Shiraz University, Shiraz, Iran.
E-mail addresses: gkarimi@engmail.uwaterloo.ca (G. Karimi);
x6li@uwaterloo.ca (X. Li).

Nomenclature

C	molar concentration (mol m^{-3})
C_f	wall friction coefficient
d_h	flow channel hydraulic diameter (m)
D	diffusion coefficient (m^2 s^{-1})
D_h	manifold hydraulic diameter (m)
E	cell or stack voltage (V)
f_{Pt}	mass ratio of platinum to carbon support
F	Faraday constant (96485 C mol^{-1})
H	bipolar plate effective height (m)
J	cell current density (A m^{-2})
K_E	electrokinetic permeability of polymer electrolyte membrane (m^2)
K_p	hydraulic permeability of polymer electrolyte membrane (m^2)
l	flow channel length (m)
ℓ_m	fraction of catalyst layer void space occupied by liquid water
L	control volume length (m)
m_{Pt}	platinum mass loading per unit electrode area (kg m^{-2})
$\dot{m}$	mass flow rate (kg s^{-1})
n	exponent used to represent frictional/minor losses
N	number of cells/loops/branches/flow channels/turns
$\dot{N}$	molar flow rate (mol s^{-1})
$\dot{N}_0$	initially assumed molar flow rate (mol s^{-1})
$\dot{N}_r$	rate of reactant consumption in the catalyst layer (mol s^{-1})
P	pressure (Pa)
P_c	compressor power (W)
r	flow resistance coefficient
R	universal gas constant (8.314 kJ kmol^{-1} K^{-1})
Re	Reynolds number
$\mathcal{S}$	stoichiometry
S_E	voltage spread (%)
T	stack temperature (K)
V	average velocity (m s^{-1})
W	bipolar plate effective width (m)

Greek letters

α	ratio of pressure loss in the bipolar flow channels to that of the manifold
δ	thickness (m)
Δ	difference
η	overpotential (V)
θ	flow direction convention (+1 for clockwise, −1 for counter clockwise)
κ_s	conductivity of catalyst layer solid phase (S m^{-1})
μ	viscosity (N s m^{-2})
ρ	density (kg m^{-3})

ρ_e^{bulk}	resistivity of electrode backing (Ω m)
ϕ	porosity

Subscripts

a	anode
bend	flow channel bends
bp	bipolar plate
branch	branch (control volume)
c	cathode/flow channel/catalyst layer
cell	fuel cell
cp	cooling plate
drag	dragged molecules
e	electrode backing
f	friction
H$^+$	protons
H$_2$	hydrogen
O$_2$	oxygen
i	loop number
in, inlet	in/inlet value
j	branch number
loop	loop
max	maximum value
min	minimum value
m	minor loss/polymer electrolyte membrane
out, outlet	out/outlet value
r	reacting
rev	reversible
stack	stack
t	total/turn

models can be found in Baschuk and Li [3,4]. The majority of these stack models are extensions of the empirical and/or mathematical PEM fuel cell models, originally developed for a single PEM fuel cell. Reactant distributions within the stack is modeled by treating the stack manifold and gas flow channels as hydraulic network, and the voltages of the cells in the stack are determined using single cell models. Generally, these models suffer from two limitations: minor losses are neglected and the stack performance is studied under a specified manifold configuration. As will be shown in this study, the minor losses have significant influence for the typical PEM fuel cell stack designs. As a result, these model predictions may not be adequately justified.

To this end, the present study formulates a PEM fuel cell stack by incorporating multiple inlet/outlet topologies and minor loss effects. The fuel and oxidant flow distributions within the stack are determined by applying the conservation of mass and energy equations to the stack flow network. Cell voltages are determined using the steady state, isothermal, single cell model developed previously by Baschuk and Li [3]. A variety of flow configurations for a fuel cell stack operating with humidified hydrogen and air are simulated,
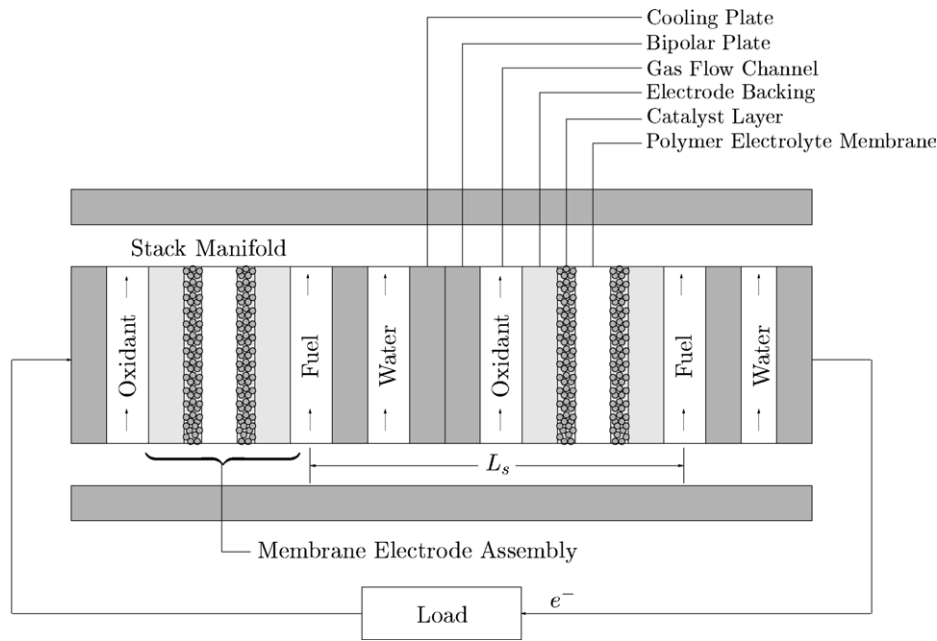
Fig. 1. Schematic illustration of a PEM fuel cell stack.

strategies for reducing the unequal distribution of reactants within the stack are examined, methods for the improvement of stack performance are described, optimization of stack design is performed, and optimal stack design is obtained.

2. Model formulation

A diagram of a typical section of a fuel cell stack is shown in Fig. 1. The individual cells, referred to as membrane electrode assemblies (MEA), are composed of a membrane electrolyte sandwiched between two porous electrodes. The MEAs produce direct current electricity. Bipolar plates, which are electrically conducting, separate the MEAs as well as provide a means for delivery of the fuel and oxidant to the catalyst layer at the electrode–membrane interface. The basic unit is repeated to build up a stack. A complete multi-cell stack may include cooling plates, which are specially designed, and similar to bipolar plates. These plates are designed to provide a uniform stack temperature.

The fuel and oxidant for each PEM fuel cell are supplied by the stack manifold, with the anode manifold supplying fuel and the cathode manifold supplying oxidant. The major component of the fuel for a PEM fuel cell is hydrogen, with carbon dioxide and carbon monoxide being present if reformate fuel is utilized. The oxidant used in a PEM fuel cell is oxygen, with nitrogen being present if air is used as the oxygen supply. The gas flow channels remove the water produced by the electrochemical reactions within the membrane electrode assembly and supply the humidity required to avoid polymer electrolyte membrane from dehydration. In addition to fuel and oxidant, water is circulated through cooling plates

in order to remove the heat produced by the PEM fuel cells and maintain a constant stack temperature.

The stack performance, often measured in terms of the stack voltage, E_{stack}, can be determined by:

$$E_{\text{stack}} = \sum_{1}^{N_{\text{cell}}} E_{\text{cell}} - \sum_{1}^{N_{\text{cell}}} \eta_{\text{cp}} \tag{1}$$

where N_{cell} is the total number of fuel cells in the stack, E_{cell} is the voltage of each cell, and η_{cp} is the ohmic loss due to a cooling plate, and is determined by treating the ohmic loss for the cooling plate similar to the ohmic loss for bipolar plate.

The stack model presented here consists of two parts: the single cell model and the stack flow network model. The single cell model determines the voltage of each cell in the stack based on the cell inlet pressure, temperature, stoichiometry, and reactant composition in the gas flow channels, as well as the current density and design parameters. The flow conditions around each cell is determined using the stack flow model.

2.1. Single cell model

The voltage of each cell in the stack is determined using the single cell model developed by Baschuk and Li (2002) [3]. According to this model, the output voltage of a single cell can be determined as follows:

$$E_{\text{cell}} = E_{\text{rev}} - \eta_{\text{a}} - |\eta_{\text{c}}| - 2\eta_{\text{bp}} - 2\eta_{\text{e}} - \eta_{\text{m}} \tag{2}$$

where E_{rev} is the reversible cell voltage, η_{a} and η_{c} are the overpotentials attributed to the anode and cathode catalyst layers, respectively. The voltage losses caused by the bipolar

plate, electrode backing and polymer electrolyte membrane are denoted by η_{bp}, η_e, and η_m, respectively.

The reversible cell voltage is the cell potential obtained at thermodynamic equilibrium. It is a function of temperature and reactant concentration through a modified version of the Nernst equation. The cell voltage is reduced from the reversible cell voltage by the overpotentials associated with the various components of the PEM fuel cell. The anode and cathode catalyst layer overpotentials are found by considering species conservation, and proton and electron migration within the catalyst layers. Proton and electron migration through the catalyst layers are related to the protonic and electrical current using Ohm's law. Species conservation requires modeling of reaction kinetics and mass transport. Oxygen reduction is modeled with the Butler–Volmer equation in the cathode catalyst layer, while in the anode catalyst layer the adsorption and desorption of H_2, CO and O_2, the electro-oxidation of the adsorbed hydrogen and carbon monoxide, and the heterogeneous oxidation of H_2 and CO by O_2 are included in the reaction kinetics. The voltage losses attributed to the bipolar plate and electrode backing are the result of electron migration; the overpotential is calculated by considering the electrode backing and bipolar plate as electrical resistances. The overpotential associated with the proton migration in the polymer electrolyte membrane is determined by the Nernst–Planck equation assuming a constant conductivity for the fully hydrated polymer electrolyte membrane.

Determination of the reversible cell voltage and overpotentials requires several operating and design parameters. Design parameters depend on the manufacture of the PEM fuel cell and include properties, such as conductivity and porosity, and geometric dimensions. The operating parameters include current density, temperature, pressure, reactant composition and stoichiometry.

Due to the series connection, the current density in each cell will be equal. The circulation of cooling water maintains a uniform temperature for each cell in the stack. However, the pressure, reactant composition and stoichiometry can vary from cell to cell if the mass flow rate and pressure distributions within the stack are unequal; this variation is analyzed with the stack flow model described in the next section.

2.2. Stack flow model

The cross-section of a PEM fuel cell stack was shown before in Fig. 1. Fig. 2 illustrates the structure of a typical bipolar plate with manifolds and three flow channels arranged in serpentine configuration. To model the flow distribution in the stack, the complex fuel and/or oxidant flow paths consisting of the stack's inlet(s), outlet, manifolds and gas flow channels can be reduced into a graphical flow network as depicted in Fig. 3. In this diagram, fuel cells are surrounded by the manifolds and flow channels. The top manifold supplies the reactants to the gas flow channels of the fuel cell stack and the gas flow channels exit into the bottom manifold.
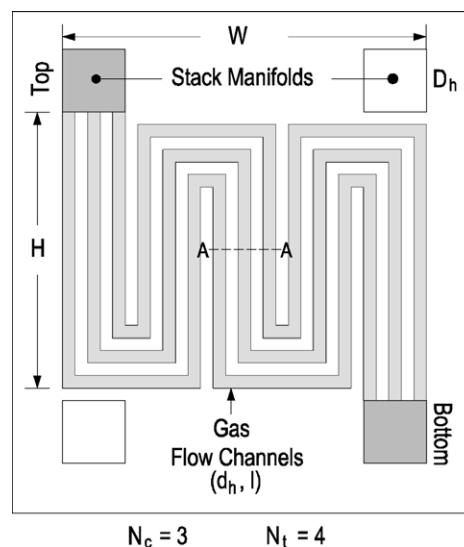

Fig. 2. Illustration of the bipolar plate with serpentine flow channel configuration with three channels per plate and four U-turns per channel.

In practice, the electrochemical reactions start at the beginning of flow channels immediately after the reactants are brought into contact with the catalyst layer. The reaction rates vary along the flow channels as the reactant composition and pressure change. However, the present network model uses a control volume approach to simplify the detailed analysis. The top and bottom manifolds are segmented to account for the flow and composition change as they interact with the flow channels. Each gas flow channel is divided into two sections or branches of identical lengths. The upstream channel starts from the top manifold and extends half way through the channels length. The downstream channel starts from the channel midpoint to the bottom manifold. The boundary between the two sections is indicated by the plane A–A in Fig. 2. It is assumed that the pressure and compositions are uniform in each control volume. Mass transfers due to electrochemical reactions are considered to take place at average operating conditions determined at the middle of the flow channels. These reaction sites are denoted by the symbol "⊗" in Fig. 3. Therefore, the simplified stack flow network consists of several loops, with each loop comprising six branches: two in the manifolds, and two in each flow channels. The interfaces at which manifold branches meet are represented by nodes as illustrated in Fig. 3.

With the present multiple inlet stack model, numerous flow configurations can be examined for optimum PEM fuel cell stack performance. The inlets supply humidified gaseous hydrogen and air (oxygen) to the anode and cathode sides, while the outlets remove the reaction product and excess reactants.

2.2.1. Conservation of mass

The inlet hydrogen and oxygen molar flow rates to the anode and cathode sides of the stack are determined by
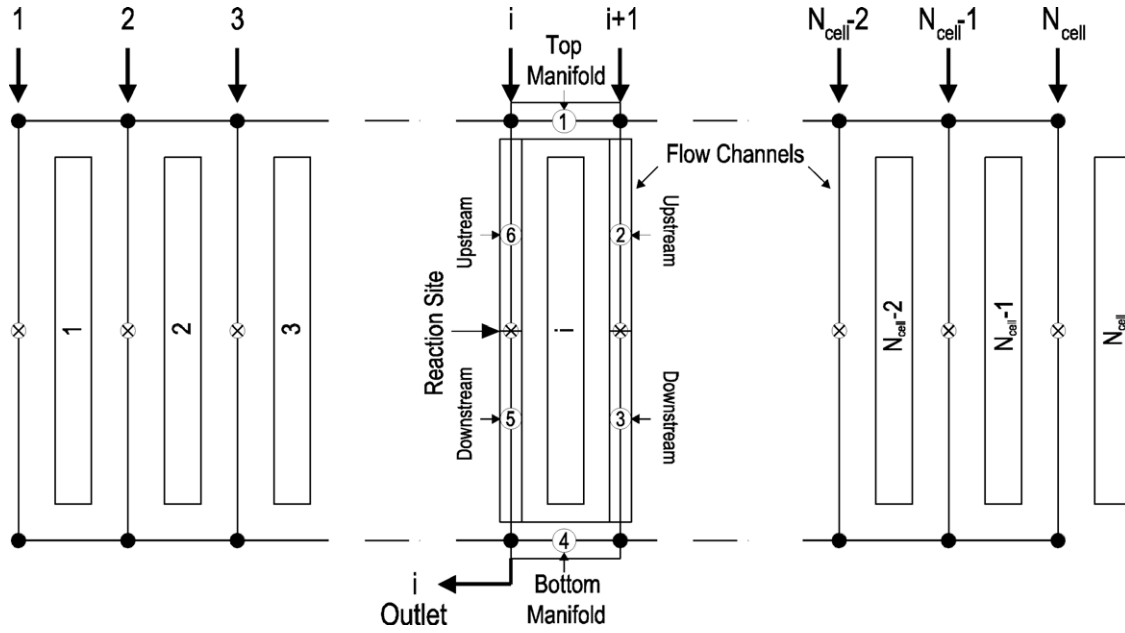
Fig. 3. Simplified flow network configuration of a PEM fuel cell.

$$\dot{N}_{H_2}^{\text{stack}} = \frac{\mathcal{S}_a N_{\text{cell}} J A_{\text{cell}}}{2F}, \qquad \dot{N}_{O_2}^{\text{stack}} = \frac{\mathcal{S}_c N_{\text{cell}} J A_{\text{cell}}}{4F}$$

where $\mathcal{S}_a$ and $\mathcal{S}_c$ are the stack anode and cathode stoichiometries, respectively. Total inlet molar flow rates can be calculated by adding the water vapor and nitrogen to the inlet streams. The maximum amount of water vapor coming into the stack with the reactants corresponds to 100% relative humidity in the incoming gas streams.

The distribution of incoming components is governed by the conservation laws. The conservation of mass principle requires that total mass flow into and out of each node in the flow network (Fig. 3) must be equal, or

$$\sum_{\text{in}} \dot{m}_t = \sum_{\text{out}} \dot{m}_t \quad \text{(for all nodes)} \tag{3}$$

The fuel and oxidant undergo electrochemical reactions during which reactants are consumed and water is produced. The amount of consumption in the anode and cathode catalyst layers differ, but in general they can be written as:

$$\Delta \dot{N}_r = \sum_{i=\text{species}} \Delta \dot{N}_r^i \tag{4}$$

where the summation is over all the species taking part in the reaction. For the anode catalyst layer, the species present are considered to be H_2 and H_2O. H_2 is the only species consumed in the anode catalyst layer. The rate of hydrogen molar consumption can be calculated using Faraday's law:

$$\Delta \dot{N}_r^{H_2} = -\frac{J A_{\text{cell}}}{2F} \tag{5}$$

where J is the current density, A_{cell} is the active area of a PEM fuel cell, and F is the Faraday constant.

The exit stream from the anode is assumed to be fully saturated with no condensed water. Since H_2 is consumed in the anode reaction sites, the excess water molecules are considered to migrate through the polymer electrolyte membrane towards the cathode side as a net result of electroosmotic drag and back diffusion. The molar consumption in the anode can be expressed as:

$$\Delta \dot{N}^{\text{Anode}} = \Delta \dot{N}_r^{H_2} + \dot{N}_{\text{drag}}^{H_2O} \tag{6}$$

where $\dot{N}_{\text{drag}}^{H_2O}$ is the net water transport from anode to the cathode through the electrolyte membrane.

In the cathode catalyst layer, the species present are O_2, N_2, and H_2O. Nitrogen does not react in the cathode catalyst layer and the amount of oxygen consumed and water produced can be calculated with Faraday's law:

$$\Delta \dot{N}_r^{O_2} = -\frac{J A_{\text{cell}}}{4F} \tag{7}$$

$$\Delta \dot{N}_r^{H_2O} = \frac{J A_{\text{cell}}}{2F} \tag{8}$$

Water molecules dragged from the anode side and those produced in the fuel cell are assumed to enter the cathode gas flow channels. Therefore, the molar accumulation in the cathode catalyst layer becomes:

$$\Delta \dot{N}^{\text{cathode}} = \Delta \dot{N}_r^{O_2} + \Delta \dot{N}_r^{H_2O} + \dot{N}_{\text{drag}}^{H_2O} \tag{9}$$

As the water content of the cathode side flow channels increases, the possibility of water molecules being liquefied there also increases. The amount of liquid water present is expressed in terms of the thermodynamic property called quality, and the thermodynamic quality in each segment of the cathode side is determined based on the reactant

compositions, local temperature and pressure, and the flow properties are modified accordingly.

2.2.2. Conservation of energy

In order to satisfy the conservation of energy, the sum of pressure changes around each of the loops, i, should be zero:

$$\sum_{j=1}^{N_{\text{branch}}} \theta_{i,j} \Delta P_{i,j} = 0 \quad (i = 1, 2, 3, \dots, N_{\text{loop}}) \tag{10}$$

where $\theta_{i,j}$ is a sign convention representing the direction of flow in the branch j of loop i. $\theta_{i,j}$ is considered to be $+1$ when fluid flows in clockwise direction and -1 if the direction is reversed. Total pressure drop in branch j of loop i is composed of frictional, $\Delta P_{f,i,j}$, and local or minor losses, $\Delta P_{m,i,j}$, and can be written in the form of

$$\Delta P_{i,j} = \Delta P_{f,i,j} + \Delta P_{m,i,j} \tag{11}$$

The frictional pressure loss can be expressed by Darcy–Weisbach equation

$$\Delta P_{f,i,j} = C_{f,i,j} \frac{L_{i,j}}{D_{h,i,j}} \frac{\rho_{i,j} V_{i,j}^2}{2} \tag{12}$$

where $L_{i,j}$ and $D_{h,i,j}$ are the branch (or control volume) length and hydraulic diameter, $\rho_{i,j}$ is the fluid average density, and $V_{i,j}$ is the average velocity in the branch j of the loop i.

The friction coefficient, $C_{f,i,j}$, is a function of the Reynolds number [5]:

$$C_{f,i,j} = \begin{cases} 16\, Re_{i,j}^{-1} & Re_{i,j} \leq 2000 \\ 0.079\, Re_{i,j}^{-1/4} & Re_{i,j} \geq 4000 \end{cases} \tag{13}$$
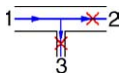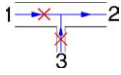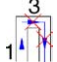
where the Reynolds number is defined based on the hydraulic diameter:

$$Re_{i,j} = \frac{\rho_{i,j} V_{i,j} D_{h,i,j}}{\mu_{i,j}} \tag{14}$$

The density and viscosity of the fluid are calculated incorporating the flow composition and operating conditions using the equations described in Baschuk and Li [3]. A linear relationship is used to calculate friction coefficient in the transition regime where the Reynolds number falls between 2000 and 4000.

Minor losses arise as a result of sudden or gradual changes in flow directions leading to the formation of a secondary recirculatory fluid motion. Unlike frictional losses, minor losses are local and occur in regions where the recirculations take place. The relative magnitude of minor to frictional losses depends primarily on the hydraulic network geometry and flow conditions. For hydraulic systems with long ducts, minor losses may be neglected. In a PEM fuel cell stack, on the other hand, the top and bottom manifold branches are short, the change in the flow direction is sudden, and the number of turns in the flow channels is large; as a result, minor losses may become *major* and should be included in the

Table 1
Branch, confluence, and bend head loss correlations [6]

$$\Delta P_{m,1-j} = k_{1-j} \frac{\rho_1 V_1^2}{2} \ (j = 2, 3), k_{1-2}$$
$$= \left[10.65 - 19.76 \left(\frac{V_2}{V_1} \right) + 11.2 \left(\frac{V_2}{V_1} \right)^2 \right]$$
$$\times \frac{10^3}{Re_2} \left(\frac{V_2}{V_1} \right)^2, k_{1-3} = \frac{7000}{Re_3} \left(\frac{V_3}{V_1} \right)^2$$

$$\Delta P_{m,2-j} = k_{2-j} \frac{\rho_2 V_2^2}{2} \ (j = 1, 3), k_{2-1}$$
$$= \frac{2100}{Re_1} \left(\frac{V_1}{V_2} \right)^2, k_{2-3} = \frac{7300}{Re_3} \left(\frac{V_3}{V_2} \right)^2$$

$$\Delta P_{\text{bend}} = 2k_{1-3} \frac{\rho V^2}{2}, k_{1-3} = \frac{7000}{Re}$$

analysis. More specifically, these so-called minor losses can be classified into three groups: (a) minor losses due to the change in the flow direction in the sharp turns/bends in the gas flow channels, and the minor losses associated with the (b) confluence and (c) branching when the flow channels are either charged from the top manifold or discharged into the bottom manifold.

Minor losses are often measured experimentally and expressed by empirical correlations. A comprehensive set of formulations for laminar-to-laminar and turbulent-to-turbulent flow regimes can be found in Jamison and Villemonte [6], Blevins [7] and Idelchik [8]. For fuel cell stack applications, although a laminar flow prevails in the flow channels over a wide range of operating conditions, a combination of turbulent-laminar flow regime change might occur at the manifold-flow channel intersections near the stack inlet(s) at large current densities. The minor loss coefficients associated with such flow regime changes have not yet been reported. Hence, the formulations given by Jamison and Villemonte [6] for laminar flow as listed in Table 1 are used in the present work. The locations of the minor losses are specified by "×" in the table. It is seen that both frictional and minor losses depend on the flow distribution in the stack.

3. Numerical procedure

Due to the non-linear relationship between the pressure losses and mass flow rates in the stack manifolds and gas flow channels, the mass flow rate and pressure distributions must be calculated using an iterative technique. The flow network solution algorithm devised in this work is based on the Hardy Cross method [9]; however, it has been extensively modified to account for the variations of pressure and composition and to include the effect of minor losses. The modified algorithm requires that all the conservation equations be written in terms of total molar flow rates. This approach simplifies tracking of all components in the different parts of the stack.

The numerical solution begins with assigning a temporary flow direction to the flow network. The sum of the molar flow rates from all the inlets (with known compositions) is then
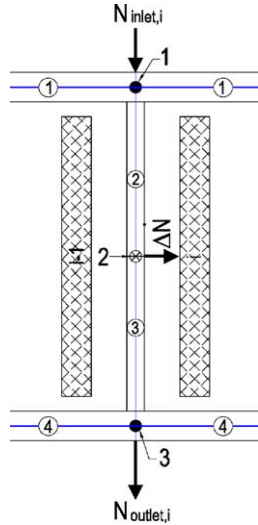
Fig. 4. Schematic illustration for nodal mass conservation.

divided uniformly among the upstream sections of all the gas flow channels. The molar flow rates and compositions in the downstream sections of the flow channels are calculated by subtracting the consumed reactants and adding the produced components. Water transport through the membrane due to the combined effects of electroosmotic drag and back diffusion is also considered (Eqs. (6) and (9)). The next step is to use the conservation of mole equation and calculate the molar flow rates in the top and bottom manifolds based on the predefined directions and the assumed molar flow rates in the flow channels. Fig. 4 illustrate three nodes in the top, middle (reaction site), and bottom of a typical flow channel. Application of the conservation of mole equation to these nodes result in total molar flow rates, $\dot{N}_t$, in branches 1 and 4 of the ith loop and branch 3 of the $(i-1)$th loop, respectively, as follows:

$$\dot{N}_{i,1} = \frac{\theta_{i-1,1}\dot{N}_{i-1,1} + \dot{N}_{\text{inlet},i} - \theta_{i-1,2}\dot{N}_{i-1,2}}{\theta_{i,1}} \qquad (15)$$

$$\dot{N}_{i-1,3} = \frac{\theta_{i-1,2}\dot{N}_{i-1,2} + \Delta\dot{N}_{i-1}}{\theta_{i-1,3}} \qquad (16)$$

$$\dot{N}_{i,4} = \frac{\theta_{i-1,3}\dot{N}_{i-1,3} - \theta_{i-1,4}\dot{N}_{i-1,4} - \dot{N}_{\text{outlet},i}}{\theta_{i,4}} \qquad (17)$$

where $\dot{N}_{\text{inlet},i}$ and $\dot{N}_{\text{outlet},i}$ are the total molar flow rates entering and leaving the stack at that particular location. A negative molar flow rate (in any of the above equations) indicates that the assumed flow direction in that branch is incorrect and must be reversed.

The conservation of energy equation must also be satisfied by the assumed molar flow rates. Eq. (10) can be expressed in terms of molar flow rates as follows:

$$\Delta P_i = \sum_{j=1}^{N_{\text{branch}}} \theta_{i,j}[r_{1,i,j}\dot{N}_{i,j}^{n1,i,j} + (r_{2,i,j} + r_{3,i,j})\dot{N}_{i,j}^{n2,i,j}] = 0$$

$$(i = 1, 2, 3, \ldots, N_{\text{loop}}) \qquad (18)$$

where the frictional and minor losses have been expressed in the form $r\dot{N}^n$. For every branch r_1 is the coefficient associated with the frictional loss, r_2 is the coefficient associated with the branch or confluence loss, and r_3 represents the coefficient for the losses in the bends of gas flow channels. The r and n parameters are obtained by rewriting Eq. (12) and the correlations listed in Table 1 on the molar flow rate basis. For instance, $r_{1,i,j}$ can be expressed as:

$$r_{1,i,j} = \begin{cases} \dfrac{0.0407 L_{i,j}\mu_{i,j}RT}{D_{\text{h},i,j}^4 P_{i,j}} & \text{(laminar)} \\[3mm] \dfrac{1.3560 \times 10^{-6} L_{i,j}\mu_{i,j}^{0.25}\rho_{i,j}^{0.75}(RT)^{1.75}}{D_{\text{h},i,j}^{4.75} P_{i,j}^{1.75}} & \text{(turbulent)} \end{cases}$$

$$(19)$$

where R is the gas constant. T is the stack operating temperature and considered to be constant throughout the stack. $P_{i,j}$ represents the absolute pressure of the branch. The value of n is equal to 1 for laminar flow and 1.75 for turbulent flow. It is seen that the value of r_1 depends exclusively on the conditions of the branch it is calculated for and independent of other branches.

Minor losses can be expressed similarly; however, unlike frictional losses, the minor loss of a branch depends not only on the flow conditions of the branch but also is influenced by the conditions of the neighboring branches. Therefore, extra care must be taken to include the influence of neighboring branches in the calculations. Table 2 is equivalent to Table 1 in which all possible minor losses are presented on molar flow rate basis. As indicated, the power of

Table 2
Branch, confluence, and head loss correlations rewritten in terms of the molar flow rate, otherwise identical with those shown in Table 1

$$\Delta P_{m,1-2} = \left[10.65 - 19.76\left(\frac{V_2}{V_1}\right) + 11.2\left(\frac{V_2}{V_1}\right)^2\right]\frac{2\mu_2\rho_1 RT}{\pi P_2\rho_2 D_{H2}^3}\dot{N}_2, \quad \Delta P_{m,1-3} = \frac{14\mu_3\rho_1 RT}{\pi P_3\rho_3 D_{H3}^3}\dot{N}_3$$

$$\Delta P_{m,1-2} = \left[10.65 - 19.76\left(\frac{V_2}{V_1}\right) + 11.2\left(\frac{V_2}{V_1}\right)^2\right]\frac{2\mu_2\rho_1 RT}{\pi P_2\rho_2 D_{H2}^3}\dot{N}_2, \quad \Delta P_{m,1-3} = \frac{14\mu_3\rho_1 RT}{\pi P_3\rho_3 D_{H3}^3}\dot{N}_3$$

$$\Delta P_{\text{bend}} = 2\Delta P_{1-3} = \frac{28\mu RT}{\pi PD_H^3}\dot{N}$$

the molar flow rates for all different minor losses is equal to 1 ($n_2 = 1$).

Although the initially assumed/calculated molar flow rates satisfy the conservation of mass, the conservation of energy may not be satisfied. Hence, the corrected molar flow rates, $\dot{N}_{i,j}$, can be related to the assumed flow rates, $\dot{N}_{i,j,0}$, as:

$$\dot{N}_{i,j} = \dot{N}_{i,j,0} + \Delta\dot{N}_i \tag{20}$$

where $\Delta\dot{N}_i$ is the correction.

For each branch, total pressure loss can be expressed as:

$$\begin{aligned}
\Delta P_{i,j} &= r_{1,i,j}(\dot{N}_{i,j,0} + \Delta\dot{N}_i)^{n_{1,i,j}} \\
&\quad + (r_{2,i,j} + r_{3,i,j})(\dot{N}_{i,j,0} + \Delta\dot{N}_i) \\
&= r_{1,i,j}(\dot{N}_{i,j,0}^{n_{1,i,j}} + n_{1,i,j}\dot{N}_{i,j,0}^{n_{1,i,j}-1}\Delta\dot{N}_i + \cdots) \\
&\quad + (r_{2,i,j} + r_{3,i,j})(\dot{N}_{i,j,0} + \Delta\dot{N}_i)
\end{aligned}$$

if $\Delta\dot{N}_i$ is small compared with $\dot{N}_{i,j,0}$, all terms of the series after the second can be dropped. The conservation of energy principle requires that for every loop i in the flow network

$$\begin{aligned}
&\sum_{j=1}^{N_{\text{branch}}} \theta_{i,j}\Delta P_{i,j} \\
&= \sum_{j=1}^{N_{\text{branch}}} \theta_{i,j}(r_{1,i,j}\dot{N}_{i,j,0}^{n_{1,i,j}} + (r_{2,i,j} + r_{3,i,j})\dot{N}_{i,j,0}) \\
&\quad + \Delta\dot{N}_i\left[\sum_{j=1}^{N_{\text{branch}}} \theta_{i,j}(n_{1,i,j}r_{1,i,j}\dot{N}_{i,j,0}^{n_{1,i,j}-1} + (r_{2,i,j} + r_{3,i,j}))\right] \\
&= 0 \quad (i = 1, 2, 3, \ldots, N_{\text{loop}})
\end{aligned} \tag{21}$$

in which $\Delta\dot{N}_i$ has been taken out of the summation because it is the same for all branches $j = 1, 2, 3 \ldots, N_{\text{branch}}$ in the loop i. Eq. (21) is solved for $\Delta\dot{N}_i$ in each loop in the network as

$$\Delta\dot{N}_i = -\frac{\sum_{j=1}^{N_{\text{branch}}} \theta_{i,j}(r_{1,i,j}\dot{N}_{i,j,0}^{n_{1,i,j}} + (r_{2,i,j} + r_{3,i,j})\dot{N}_{i,j,0})}{\sum_{j=1}^{N_{\text{branch}}} \theta_{i,j}(n_{1,i,j}r_{1,i,j}\dot{N}_{i,j,0}^{n_{1,i,j}-1} + (r_{2,i,j} + r_{3,i,j}))}$$

$$(i = 1, 2, 3, \ldots, N_{\text{loop}}) \tag{22}$$

With the initial guesses for the flow distributions, it is expected to have nonzero molar flow rate corrections. Hence, the numerical solution proceeds as follows: the values of $\Delta\dot{N}$'s are calculated for all the loops in the flow network and the molar flow rates are modified accordingly. For the branches shared by two successive loops, the correcting molar flow rates from both loops must be accounted for. The iterations are continued until convergence is reached. For the present study convergence is considered to have been reached if the maximum of ΔP's for all the loops is less than 1 Pa, as shown below:

$$\text{Maximum}(|\Delta P_i|, i = 1, 2, 3, \ldots, N_{\text{loops}}) \leq 1\,\text{Pa} \tag{23}$$

The solution of the stack flow network model provides the molar flow rate distributions, composition and pressure in the flow channels. These values are used by the single cell model to calculate E_{cell} (and η_{cp}) for each cell. Finally, the stack voltage is obtained by Eq. (1).

4. Results and discussion

The input parameters for the fuel cell and stack flow model are classified as operating and design parameters. The design parameters are the fuel cell size, stack manifold and flow channel dimensions and configuration. Operating parameters include the stack current density, temperature, pressure, stoichiometry and the reactant composition at the stack inlet. Table 3 lists a summary of the operating and relevant design parameters for various cell and stack components such as the bipolar plate, electrode backing, catalyst layer and polymer electrolyte membrane.

Fig. 5 shows the effect of minor losses on the pressure distributions along the top and bottom manifolds of a U-configuration PEM fuel cell stack as shown in Table 5 (Run #1 without minor losses and Run #2 with minor losses). The stack consists of 51 cells and operates at 5000 A m^{-2}. Fig. 5(a) and (b) shows the pressure distributions for the anode and cathode sides of the stack without considering the minor losses. The inlet pressures are at the highest and drop

Table 3

Parameters and properties used in the present PEM fuel cell stack simulations

Component	Parameter	Value
Bipolar plate	W	0.12 m
	H	0.12 m
	l	0.3–4.8 m
	d_h	5×10^{-4} to 2×10^{-3} m
	N_c	1–10
	N_t	3–40
Electrode backing[a]	ρ_e^{bulk}	$6 \times 10^{-5}\,\Omega$ m
	δ_e	2.5×10^{-4} m
	ϕ_e	0.4
Catalyst layer[a]	δ_c	2.0465×10^{-5} m
	m_{Pt}	0.004 kg m^2
	f_{Pt}	0.2
	ℓ_m	0.9
	κ_s	72700 S m^{-1}
Polymer electrolyte membrane[a]	δ_m	1.64×10^{-4} m
	K_E	7.18×10^{-20} m^2
	K_p	1.8×10^{-18} m^2
	$C_{\text{H+}}$	1200 mol m^{-3}
	$D_{\text{H+}}$	4.5×10^{-9} m^2 s^{-2}
Stack	N_{cells}	51
	N_{inlets}	1–3
	T	353 K
	P_{out}	1 atm
	J	1000–10000 A m^{-2}
	$\mathcal{S}_a$	1.2
	$\mathcal{S}_c$	2.0

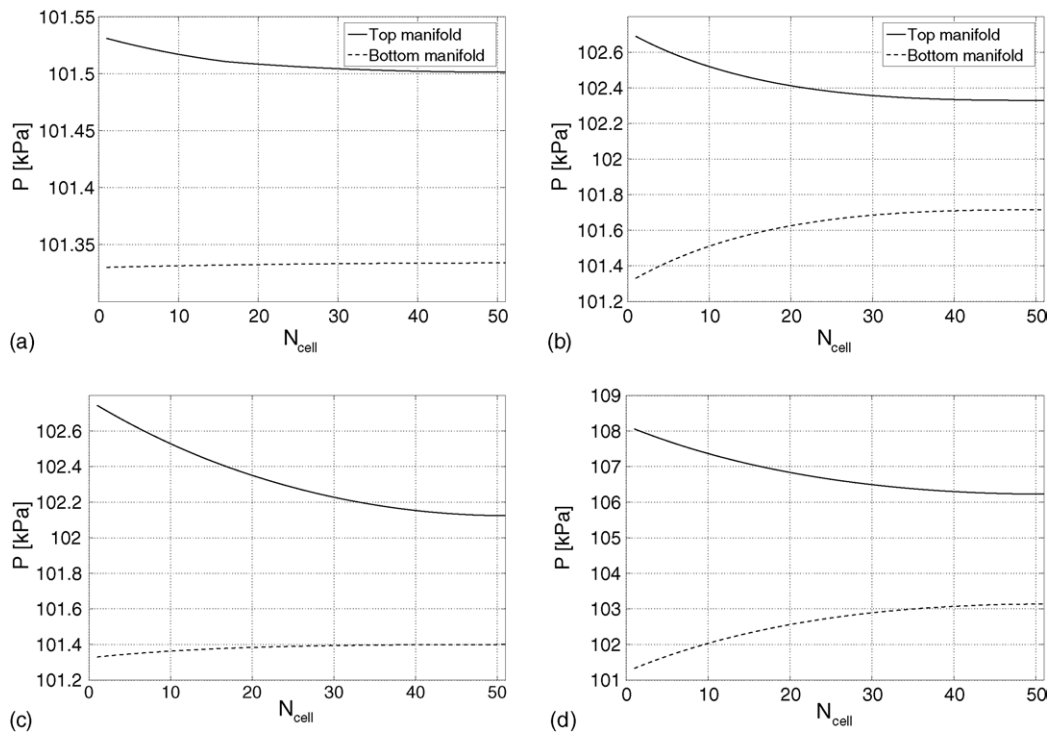[a] Parameters associated with the single cell model [3].

Fig. 5. Effect of minor losses on the pressure distributions in a U-configuration stack: (a and b) anode and cathode sides' pressure distributions without the minor losses, and (c and d) anode and cathode sides' pressure distributions with the minor losses (Runs #1 and #2: $D_h = 0.01$ m, $d_h = 0.002$ m, $l = 0.3$ m, $N_c = 10$, $N_t = 3$ and $J = 5000$ A m^{-2}).

gradually along the manifolds as flows are discharged into the flow channels. Significant pressure drops occur within the flow channels as reactants pass through the tiny channels. The unreacted components are then exited into the bottom manifold, collected channel by channel, and exit the stack at atmospheric pressure. Fig. 5(c) and (d) shows the effects of minor losses on the pressure distributions in the anode and cathode sides. With the minor losses present, larger inlet pressures are required to drive flows in the stack. Numerical results indicate that the minor-to-frictional loss ratios are in the order of 4 for both anode and cathode sides of the stack. Since the flow and pressure distributions within the stack are strongly coupled, it is therefore expected that minor losses play an important role in the stack performance.

Essentially, a large pressure drop in the manifolds may lead to uneven gas flow distribution in the stack. Uneven flow distribution causes a low reactant concentration in some of the cells and degrades the performance of these cells, hence the overall performance of the stack. On one hand, if the pressure drop in the flow channels on the bipolar plates is large, the manifold behaves like a plenum leading to a more
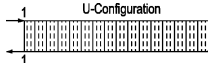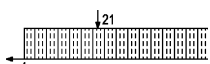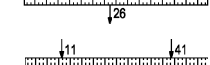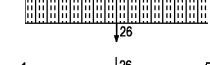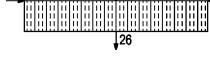
uniform reactant and hence stack voltage distributions. The large pressure drop, on the other hand, puts extra load on the air compressor. Therefore, the ratio of the pressure loss in the flow channels to that of the manifold, herein after denoted by α, is a good indication of how the flow is distributed throughout the stack and how the stack performs in general. The value of α is particularly important at the oxidant/cathode side since the resistance of flow of hydrogen is very low due to the low flow rate involved and therefore hydrogen pressure losses are usually insignificant.

Table 4 summarizes the pressure data from Fig. 5 and lists the α values for comparison. As indicated in this table, without considering minor losses, this ratio is much larger for the anode side than that of the cathode side. Hence a more uniform flow distribution is expected to prevail in the anode side of the stack. However, when the minor losses are included, the ratio decreases considerably for the anode side and only a little for the cathode side. As a result, the presence of minor losses degrades the flow distribution in the anode side without affecting significantly the flow distribution in the cathode side. This is illustrated in Fig. 6(a) and (b) where

Table 4
Relative magnitudes of the frictional and minor losses in different sections of a U-configuration stack operating at 5000 A m^{-2}

ΔP (Pa)	Manifolds			Flow channels			Stack	
	Frictional	Minor	Total	Frictional	Minor	Total	α_f	α_t
Anode	30	591	621	184	846	1030	6.17	1.6
Cathode	360	1472	1833	939	3735	4674	2.60	2.5

Table 5
Stack performance for a variety of stack configurations operating at $5000\,A\,m^{-2}$

Run no.	Stack configuration	ΔP (Pa)	P_c (W)	E_{stack} (V)	S_E (%)
1[a]	U-Configuration	797	2.6	26.0	4.2
2	U-Configuration	4182	13.4	26.1	4.6
3		4188	13.4	26.2	3.1
4		4189	13.5	26.2	2.4
5		4188	13.5	26.2	1.7
6		4186	13.4	26.2	1.2
7	Z-Configuration	4184	13.4	26.2	1.2
8		4239	13.7	26.2	1.1
9		4231	13.7	26.2	0.4
10		4237	13.7	26.2	0.6
11		4238	13.7	26.2	1.0
12		4234	13.7	26.2	0.5
13		4185	13.4	26.2	2.3

Runs #1 and #2 are identical except that the minor losses are not considered for Run #1 and included in Run #2.
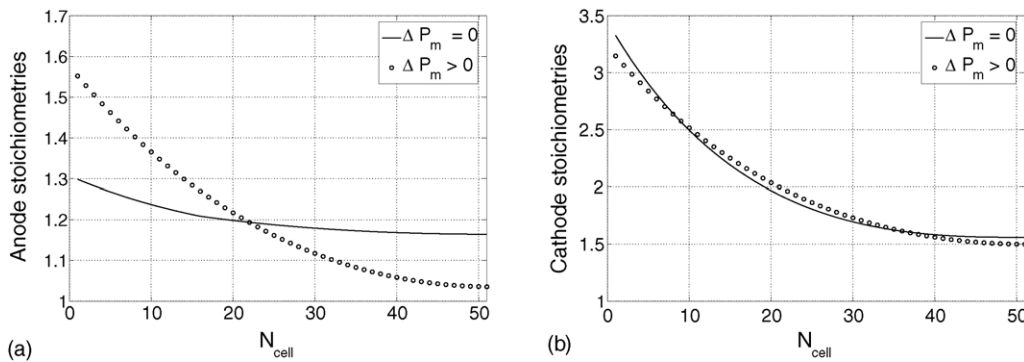
[a] $\Delta P_m = 0$.

Fig. 6. Effect of minor losses on the stoichiometry distributions in a U-configuration stack: (a) anode stoichiometry and (b) cathode stoichiometry (Runs #1, #2: $D_h = 0.01\,m$, $d_h = 0.002\,m$, $l = 0.3\,m$, $N_c = 10$, $N_t = 3$ and $J = 5000\,A\,m^{-2}$).
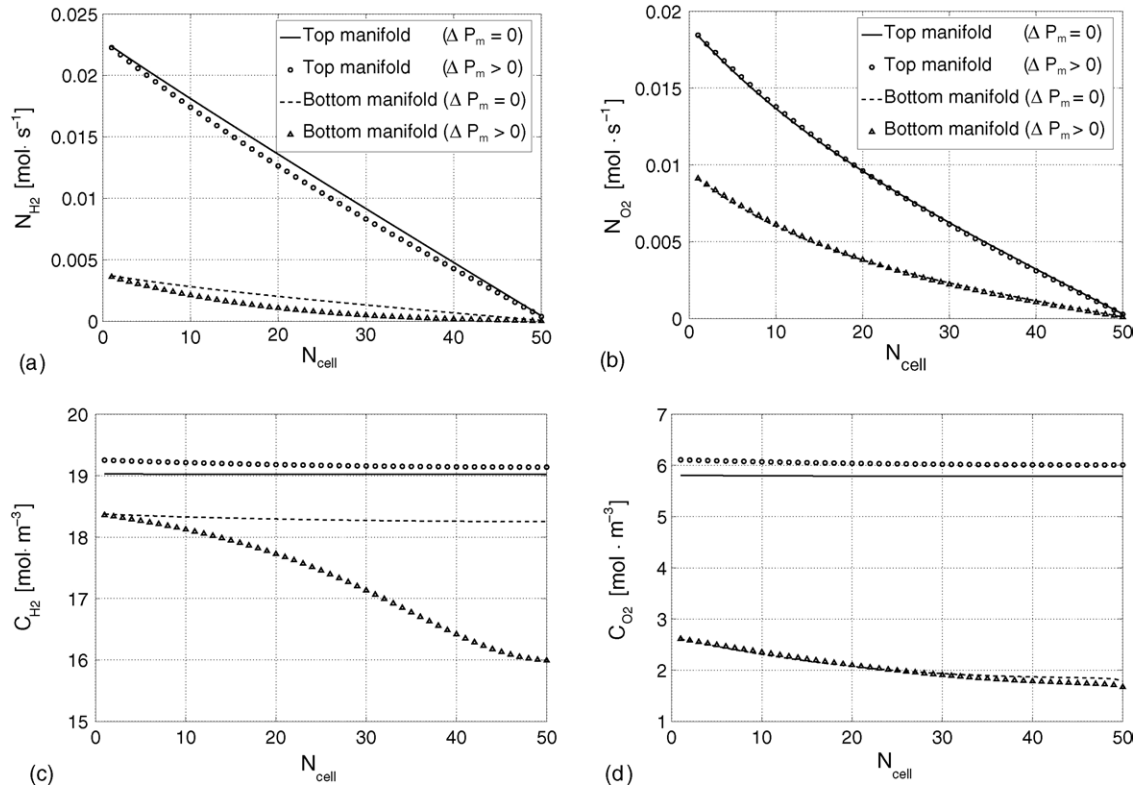
Fig. 7. Variations of molar flow rates and concentrations in the top and bottom manifolds of anode and cathode flow networks. (a and c) Variation of $\dot{N}_{H_2}$ and C_{H_2} in the anode side of the stack, and (b and d) variation of $\dot{N}_{O_2}$ and C_{O_2} in the cathode side of the stack, respectively (Runs #1 and #2: $D_h = 0.01$ m, $d_h = 0.002$ m, $l = 0.3$ m, $N_c = 10$, $N_t = 3$ and $J = 5000$ A m^{-2}).
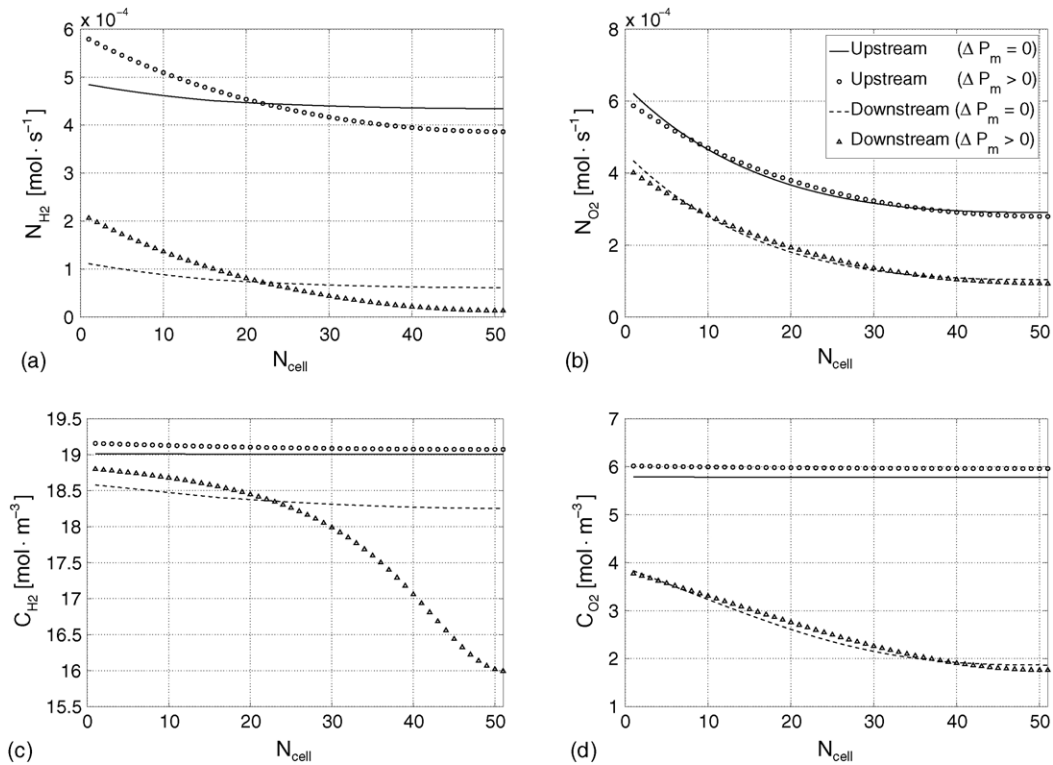

Fig. 8. Variations of molar flow rates and concentrations in the upstream and downstream flow channels of anode and cathode flow networks. (a and c) Variation of $\dot{N}_{H_2}$ and C_{H_2} in the anode side of the stack, and (b and d) variation of $\dot{N}_{O_2}$ and C_{O_2} in the cathode side of the stack, respectively (Runs #1 and #2: $D_h = 0.01$ m, $d_h = 0.002$ m, $l = 0.3$ m, $N_c = 10$, $N_t = 3$ and $J = 5000$ A m^{-2}).

cell-to-cell stoichiometry distributions are plotted for anode and cathode sides, respectively.

Fig. 7 displays the fuel and oxidant molar flow rate and concentration distributions in the top and bottom manifolds of the anode and cathode sides of the stack. The effect of minor losses on the distributions are also included in the figure. As shown in Fig. 7(a) and (b), the H_2 and O_2 molar flow rates are maximum at the stack inlet and decrease along the top manifold as the flow channels are fed with the reactants. A similar trend is observed in the bottom manifold as unreacted components along with the product water are collected from the flow channels towards the stack outlet. The concentration profiles calculated based on the control volumes' molar volumetric flow rates are shown for H_2 and O_2 in Fig. 7(c) and (d), respectively. It is evident from these figures that the effect of minor losses is more significant for the anode side of the stack as just pointed out earlier.

The effect of minor losses on the fuel and oxidant molar flow rates and concentration distributions in the upstream and downstream flow channels are shown in Fig. 8. Again, it is seen that the presence of minor losses has an adverse effect on the flow distribution in the anode side and minimal influence on the distributions in the cathode side.

The logarithmic average of reactant concentrations along with the pressure distributions in the stack flow channels are used in the single cell model to calculate stack voltage distributions for the U-configuration. Stack temperature is considered to be constant at $80\,°C$. Fig. 9 shows how the resulting voltage varies from one cell to another. As indicated in this plot, the cell voltage is maximum near the stack inlet and decreases as the distance from the inlet increases. The presence of the minor losses in the system tends to modify the voltage distribution and increase the cell-to-cell voltage variation. The cell-to-cell voltage variation can be quantified by the voltage spread of the stack defined as

$$S_E = \frac{E_{cell}^{max} - E_{cell}^{min}}{\frac{1}{N_{cell}}\sum_1^{N_{cell}} E_{cell}} \times 100\% \qquad (24)$$
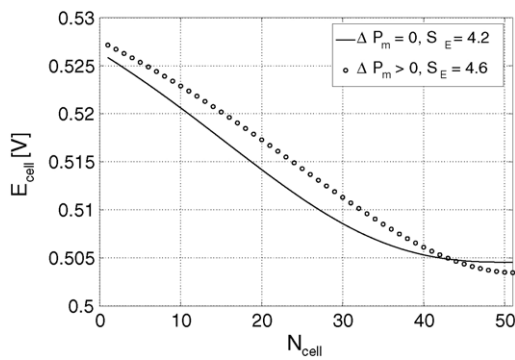

Fig. 9. Cell-to-cell voltage distributions in the U-configuration stack (Runs #1 and #2: $D_h = 0.01\,m$, $d_h = 0.002\,m$, $l = 0.3\,m$, $N_c = 10$, $N_t = 3$ and $J = 5000\,A\,m^{-2}$).
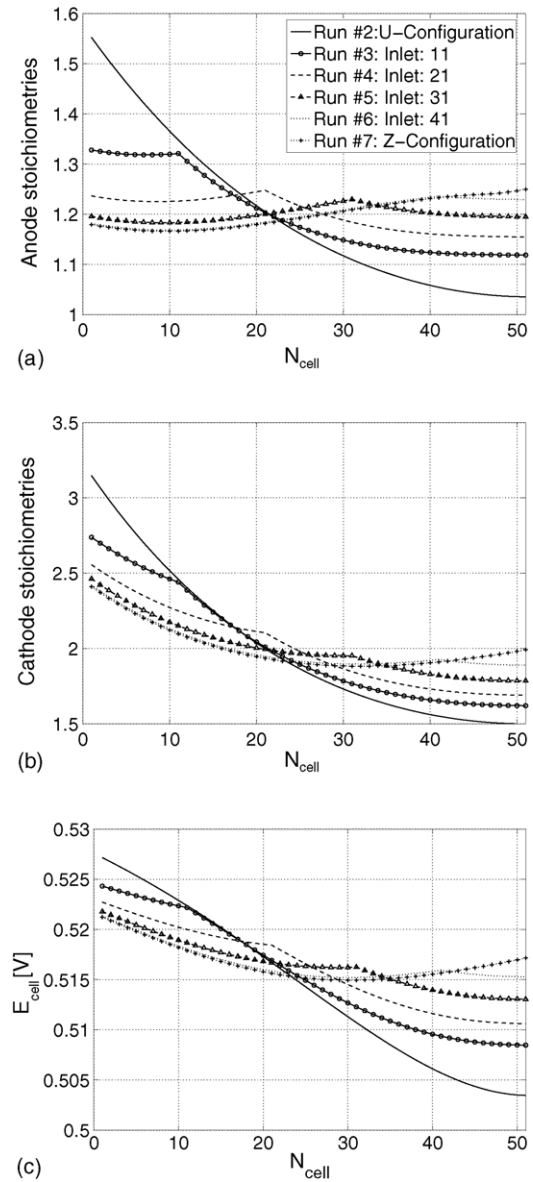

Fig. 10. Effect of inlet location on the (a) anode stoichiometry, (b) cathode stoichiometry, and (c) cell-to-cell voltage distributions (Runs #2 to #7: $D_h = 0.01\,m$, $d_h = 0.002\,m$, $l = 0.3\,m$, $N_c = 10$, $N_t = 3$ and $J = 5000\,A\,m^{-2}$).

where E_{cell}^{max} and E_{cell}^{min} are the maximum and minimum cell voltages, respectively, within the stack. For the present U-configuration and operating conditions, the voltage spread is increased by about 10% from 4.2% without considering system minor losses to 4.6% when minor losses are taken into account. This figure also shows that a slightly larger stack voltage (about 0.3%) is achieved when minor losses are taken into account.

High voltage spread is an indication of stack poor performance. In practice, a low voltage spread, uniform cell-to-cell performance, and low energy loss due to the pressure drops are desirable in order to maximize stack performance. Therefore, it is very helpful to examine other stack configurations
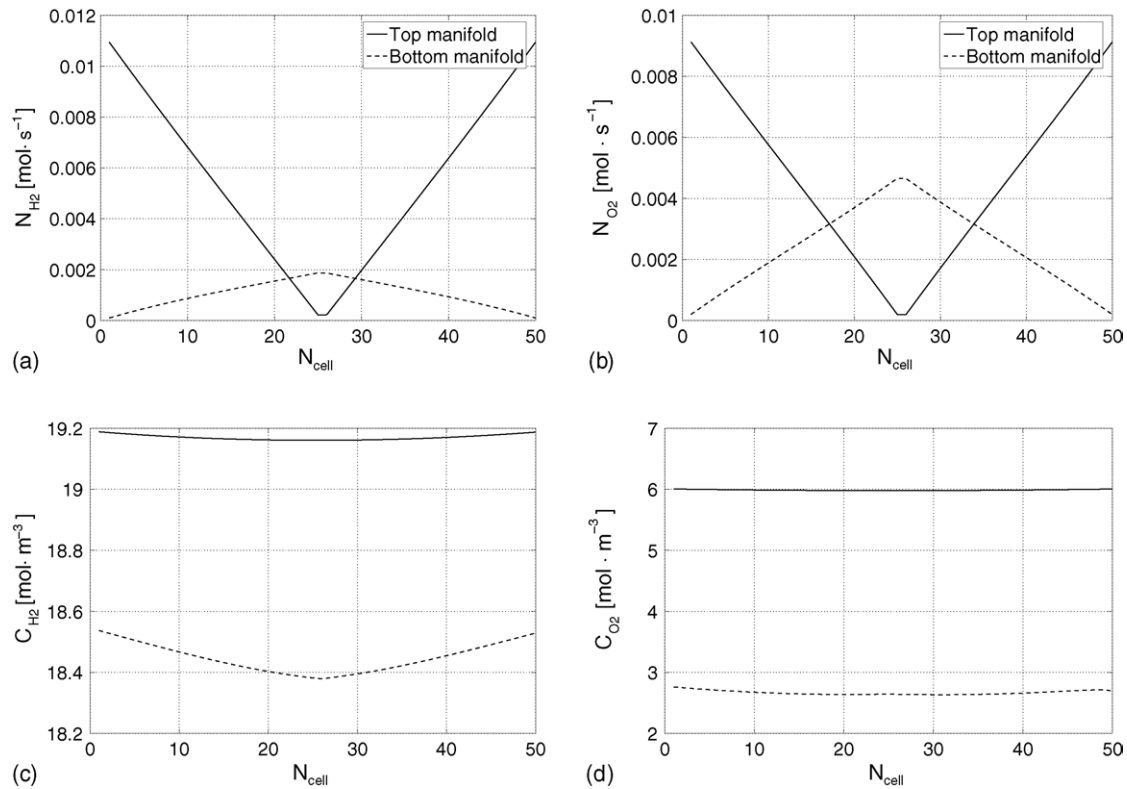
Fig. 11. Variations of (a) $\dot{N}_{H_2}$, (c) C_{H_2} in the top and bottom manifolds of the anode side and (b) $\dot{N}_{O_2}$, and (d) C_{O_2} in the top and bottom manifolds of the cathode side of a symmetric double inlet stack (Run #9: $D_h = 0.01$ m, $d_h = 0.002$ m, $l = 0.3$ m, $N_c = 10$, $N_t = 3$ and $J = 5000$ A m^{-2}).

to study the effect of inlet and outlet locations, the effect of number of inlets, and bipolar flow channel design conditions on the PEM fuel cell stack performance.

With minor losses considered, the stack inlet is moved from the present location (U-configuration) towards the stack other end-plate (Z-configuration) and the resulting anode and cathode side stoichiometries and cell-to-cell voltage distributions are calculated. Fig. 10(a) and (b) depicts variations in the anode and cathode stoichiometries as functions of the inlet location. The resulting voltage distributions are displayed in Fig. 10(c). It is clear from these figures that all the dis-

tributions are improved by moving the inlet away from the outlet. When inlet is placed close to, or at the opposite side of the outlet (e.g. Z-configuration), the PEM fuel cell stack operates with the minimum voltage spread. This is in agreement with the results recently reported by Baschuk and Li [4] in the absence of minor losses. Other stack configurations with variant inlet/outlet topologies were examined and the numerical results are summarized in Table 5. In this table, in addition to the stack voltage data, the average pressure drops for the cathode side of the stack and representative compressor power requirements for the oxidant supply, P_c, are also
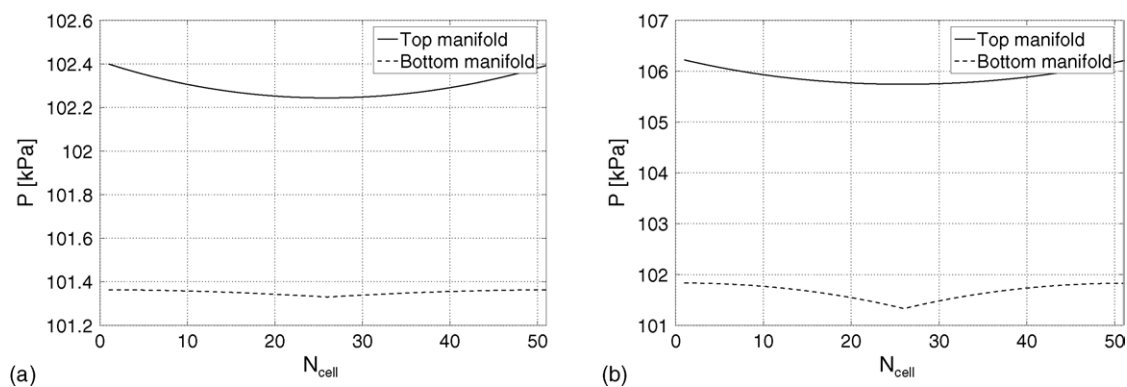

Fig. 12. Pressure distributions along the top and bottom manifolds of the symmetric double inlet stack: (a) anode side, and (b) cathode side (Run #9: $D_h = 0.01$ m, $d_h = 0.002$ m, $l = 0.3$ m, $N_c = 10$, $N_t = 3$ and $J = 5000$ A m^{-2}).
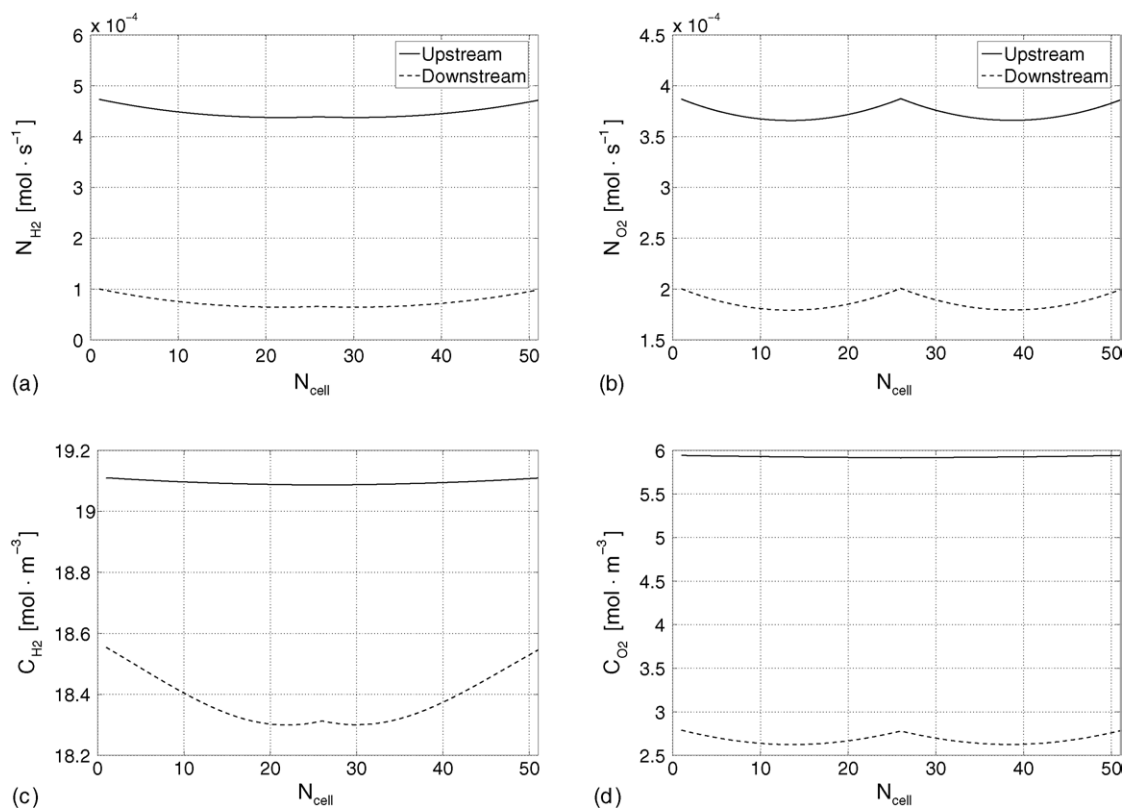
Fig. 13. Variations of (a) $\dot{N}_{H_2}$ and (c) C_{H_2} in the upstream and downstream flow channels of the anode side and (b) $\dot{N}_{O_2}$ and (d) C_{O_2} in the upstream and downstream flow channels of the cathode side of a symmetric double inlet stack (Run #9: $D_h = 0.01$ m, $d_h = 0.002$ m, $l = 0.3$ m, $N_c = 10$, $N_t = 3$ and $J = 5000$ A m^{-2}).

calculated for different configurations. It is evident from this table that a two-inlet configuration (Run #9) leads to the lowest voltage spread. Hence this configuration has been chosen for further investigations.

Fig. 11(a) and (b) depicts variations of fuel and oxidant molar flow rates in the manifolds of the anode and cathode sides, respectively. The reactants molar flow rates are decreased linearly from the inlets (located in both end-plates) towards the manifold midpoint indicating even molar distributions in the flow channels. Electrochemical reaction occurs at the reaction site of each cell, and the unreacted components and the reaction product are collected from the flow channels and accumulated as they move towards the stack outlet(s) at the center of the stack. The corresponding H_2 and O_2 concentration profiles calculated in the control volumes along the manifolds are displayed in Fig. 11(c) and (d).

The pressure variation in the stack plays an important role in the flow distributions in the flow channels. Fig. 12(a) and (b) illustrate how the pressure varies along the anode and cathode top and bottom manifolds. Careful examination of pressure data indicates that the flow channel-to-manifold pressure drop ratios, α, is about 6.2 and 9.2 for the anode and cathode sides, respectively. The large α values for the symmetric double-inlet stack configuration (as compared with 1.6 and 2.5 for U-configuration in Table 4) is a good indication of uniformity in the flow distribution and verifies the linear drop

in the molar flow rates in the anode and cathode manifolds as shown in Fig. 11(a) and (b). The corresponding fuel and oxidant molar flow rates and concentration distributions are shown in Fig. 13. As seen in these figures, the symmetric double inlet configuration forces the fuel and oxidant molar flow rates and concentrations to increase in the stack midpoints as shown in Fig. 13(a) and (b). As a result, more uniform fuel and oxidant concentrations are formed in the stack as indicated in Fig. 13(c) and (d), respectively.

The sizing optimization of the bipolar flow channels for a given basic geometry is a complex task in which several requirements must be balanced. The issue generally requires more consideration on the cathode side. The optimization of channels is not very thoroughly discussed in the literature. Some general issues, however, can be outlined. In the present study, the effects of the manifold and flow channel design conditions are studied for the two-inlet stack and bipolar plate configuration illustrated previously in Fig. 2.

Fig. 14(a) shows the strong effect of manifolds' hydraulic diameter on the cathode pressure loss ratio. For $D_h \geq 0.01$ m the ratio (α) increases considerably such that the top manifold behaves like a plenum, and distributes reactants uniformly into the flow channels. As a result, cell-to-cell voltage distribution becomes more uniform as displayed in Fig. 14(b). However, if $D_h \leq 0.005$ m, the pressure drop in the
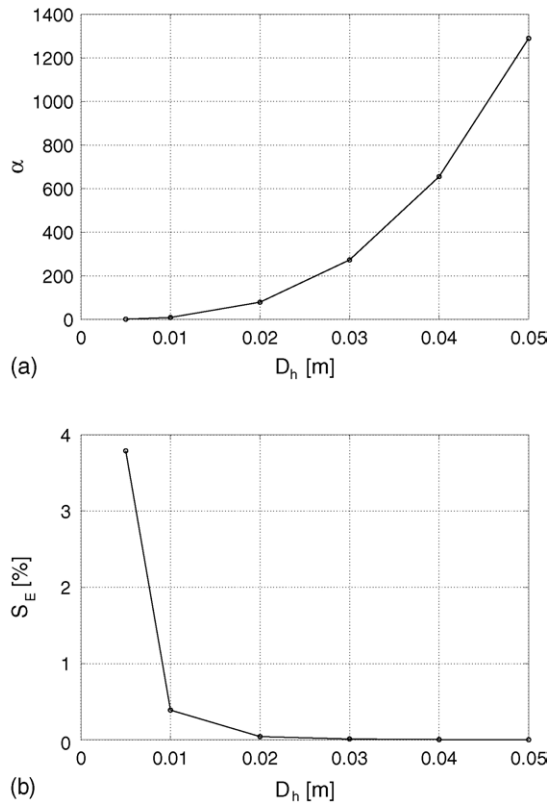
Fig. 14. Variation of (a) α, and (b) voltage spread as functions of manifolds hydraulic diameters in a symmetric double inlet stack ($d_h = 0.002$ m, $l = 0.3$ m, $N_c = 10$, $N_t = 3$ and $J = 5000$ A m^{-2}).

top manifold is comparable with (or even less than) that of flow channels, leading to a larger voltage spread. Numerical results indicated that enlarging the manifold diameter does not change significantly the energy requirement of the stack (e.g. compressor power) hence it can be concluded that a hydraulic diameter between 0.01 m and 0.02 m is optimum for which the least voltage spread is achieved at minimum compressor power requirement.

Numerical results have also provided some guidelines for bipolar plate design. The effect of number of flow channels per bipolar plate of the cathode side on the stack perfor-
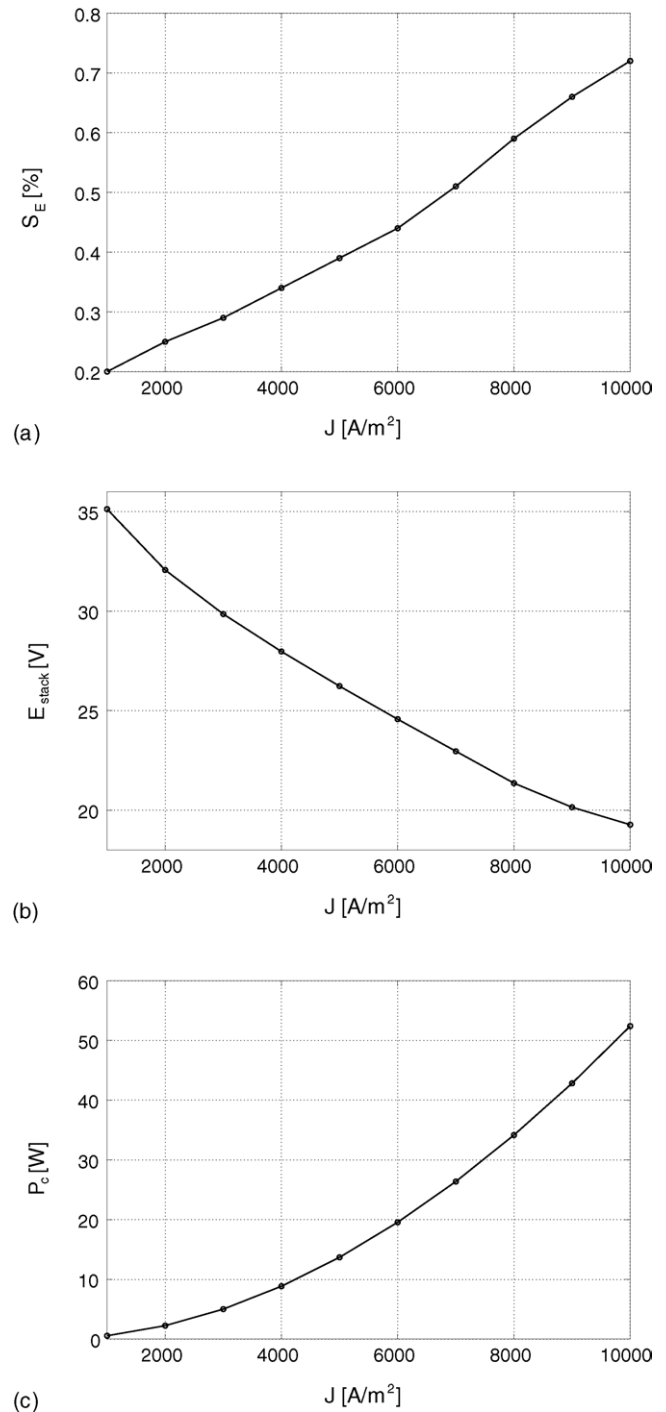

Fig. 15. Variations of (a) voltage spread, (b) stack voltage and (c) estimated power requirement for oxidant supply as functions of current density for a symmetric double inlet stack ($D_h = 0.01$ m, $d_h = 0.002$ m, $l = 0.3$ m, and $N_c = 10$, $N_t = 3$).

mance are indicated in Table 6. The flow channel diameter, d_h, length, l_c, number of flow channels, N_c and number of turns, N_t are all related (Fig. 2). If the number of flow channels is decreased, the flow channel length(s) and the number of turns must be increased (to cover the same transport area) both of which augment the minor and frictional losses in the

Table 6
Effect of bipolar design parameters on the performance of a double-inlet stack operating at 5000 A m^{-2}

Manifolds, D_h (m)	Bipolar Plate				Stack			
	N_c	N_t	l (m)	d_h (m)	α	S_E (%)	E_{stack} (V)	P_c (W)
0.01	10	3	0.30	0.002	9	0.390	26.2	14
0.01	10	4	0.48	0.001	139	0.054	27.2	127
0.01	8	5	0.60	0.001	178	0.047	27.3	147
0.01	6	7	0.72	0.001	242	0.040	27.6	174
0.01	4	10	1.20	0.001	387	0.032	28.0	219
0.01	2	20	2.40	0.001	1488	0.019	30.1	370
0.01	1	40	4.80	0.001	3254	0.011	31.6	447

bipolar plate. Although the increased pressure loss in the gas flow channel improves the stack voltage distribution and reduces voltage spread and helps to remove water droplets in the stack, its obvious drawback is that the system efficiency is reduced because the power consumption of the air supply is increased as indicated in the table. Numerical results indicate that for small number of flow channels the stack voltage spread remains close to zero.

The stack performance is also affected by the cell's current density. Fig. 15(a) and (b) shows that the voltage spread increases and the stack voltage decreases as the current density is increased. The system pressure drop and the power requirement increase at higher current densities, since larger reactant molar flow rates are now fed into the stack. Variation of the power requirement versus the current density is shown in Fig. 15(c).

5. Conclusions

The performance of a PEM fuel cell stack consisting of 51 active cells, with various inlet–outlet configurations, was studied under various design and operating conditions. Molar flow rate and pressure distributions in the stack manifolds and gas flow channels are determined using a modified version of Hardy Cross method. Minor losses due to the sharp turns in the flow channels and confluence/branching flows at the manifold-flow channel intersections are considered. The results of the flow network analysis were used in a single cell model previously developed to evaluate the stack performance. From the numerical results, the following conclusions can be made. Minor losses increase the stack operating pressure and the compression load and alter the voltage spread in the stack. The inlet–outlet configuration plays an important role in the stack performance. Although a Z-configuration stack is preferable to U-configuration, simulation results have revealed that a symmetric double inlet–single outlet topology provides excellent performance with reasonably low compressor requirement demand and minimum voltage spread. The stack performance can also be quantified by the bipolar plate-to-manifold pressure loss ratio, α. For α values of greater than 10, the stack voltage spread of less than 1% can be achieved. The size and the number of flow channels carved on the bipolar plate are also very important. Flow channels with smaller cross-sectional area and longer lengths increase the compressor power demands considerably without improving the stack voltage spread appreciably.

References

[1] I. Bar-On, R. Kirchain, R. Roth, J. Power Sources 109 (1) (2002) 71–75.
[2] P. Costamagna, S. Srinivasan, J. Power Sources 102 (1–2) (2001) 253–269.
[3] J.J. Baschuk, X. Li, Int. J. Global Energy Issues 20 (3) (2003) 245–276.
[4] J.J. Baschuck, X. Li, Int. J. Energy Res. 28 (2004) 697–724.
[5] F. White, Fluid Mechanics, 3rd ed., McGraw-Hill, New York, 1994.
[6] D.K. Jamison, J.R. Villemonte, ASCE J. Hydraulics 97 (1970) 1045–1063.
[7] R.D. Belvins, Applied Fluid Dynamics Handbook, Van Nostrand, New York, 1984.
[8] I.E. Idelchik, Handbook of Hydraulic Resistance, 3rd ed., CRC Press, Boca Raton, 1994.
[9] H. Cross, Univ. Illinois Bull. 286 (1936).